coatings

MDPI

Article

An In Vitro Investigation of Gas and Dye Leakage at the Implant–Abutment Junction Using Titanium and Cobalt Chrome-Based Abutments

Amylia Kesha Bal [1,*], Terry Richard Walton [1], Hedi Verena Kruse [1,2] and Dale Geoffrey Howes [1]

[1] Department of Oral Rehabilitation, Division of Prosthodontics, Sydney Dental School, Faculty of Medicine and Health, The University of Sydney, Sydney, NSW 2000, Australia
[2] Arto Hardy Family Biomedical Innovation Hub, Chris O'Brien Lifehouse, Camperdown, NSW 2050, Australia
* Correspondence: amylia.bal@sydney.edu.au

Abstract

The lack of integrity at the implant–abutment junction (IAJ) contributes to problems such as micromovements and microbial colonisation. This study aimed to (1) design a protocol for assessing microleakage at the IAJ using chromophore analysis not previously reported for this specific application, (2) compare gas and dye leakage between titanium (Ti) and cobalt chrome (CoCr) abutments, and (3) assess the effect of gold (Au) gilding on sealing. Forty abutments were divided into five groups: milled Ti (MTi); cast CoCr (CCoCr); milled CoCr (MCoCr); cast CoCr with Au gilding (CCoCrG); and milled CoCr with Au gilding (MCoCrG). Samples were subjected to internal pressure within a gas and dye reservoir. Chromophore analysis via UV-Vis spectrometer was used to calculate crystal violet leakage concentrations. Scanning electron microscopy (SEM) revealed close adaptation in the MTi and MCoCr groups, contrasting with irregularities in the CCoCr groups. Correspondingly, gas leakage and dye leakage were most prevalent in the CCoCr group. Fisher exact test demonstrated a statistically significant difference ($p = 0.026$) between the MCoCr and CCoCr abutments. While CCoCr exhibited the highest failure rate (62.5%), Au gilding demonstrated a trend toward reduced leakage (25% failure rate), though this did not reach statistical significance ($p = 0.315$). This chromophore analysis represents a viable and objective assessment of IAJ integrity.

Keywords: external hexagon implants; implant–abutment junction; implant–abutment connection; microgap; gold gilding; leakage

Academic Editor: Simona Liliana Iconaru

Received: 9 February 2026
Revised: 15 March 2026
Accepted: 19 March 2026
Published: 22 March 2026

1. Introduction

Dental implants offer a reliable solution for replacing missing teeth with high success rates [1,2]. However, the longevity of these restorations depends on a secure and well-fitting connection between the implant and abutment. A microgap at this interface can act as a conduit for bacteria and bacterial by-products, potentially triggering inflammatory sequelae and peri-implantitis, ultimately leading to implant failure [3–6].

Much research has explored various strategies to improve the fit and seal at the implant–abutment junction (IAJ). These include modifications of implant connection geometry [7–9], the application of computer-aided design/computer-aided manufacture (CAD/CAM) [10], the selection of different abutment materials [10] and the use of sealing agents [11,12].

The abutment material and fabrication method have an impact on the size and behaviour of the microgap. The lost-wax technique is highly technique-sensitive, relying on the skill of the technician and the quality of the alloy used [13]. In contrast, CAD/CAM technology offers greater precision and consistency, facilitating a more uniform connection between the abutment and the implant, thereby optimising the fit at the IAJ [14]. Titanium (Ti) and gold (Au) were historically the preferred abutment materials. However, the high cost of Au has led to the development of alternatives such as zirconia (Zi) and cobalt chrome (CoCr), which, in addition to Ti, are now widely used. CoCr has emerged as a viable option due to its affordability and versatility. It can be both cast and milled, making it a flexible choice for implant restorations.

Electrodepositing Au onto the fitting surface of high-Au-content alloy abutments has been shown to improve the integrity of the IAJ connection under load. A study has demonstrated that this technique can help maintain marginal bone levels over time [2]. The ductility of electrodeposited Au facilitates plastic deformation during screw clamping, allowing the abutment to conform more closely to the implant's mating geometry. This can help reduce the misfit caused by machining or casting discrepancies, potentially enhancing the sealing against microleakage and improving joint stability [15–17].

The misfit at the IAJ is typically documented through measurements under scanning electron microscopy (SEM) of the external perimeter. However, it has been shown that inter-observer subjectivity and optical measurement variability may significantly affect these measurements [15]. In addition, the presence of misfit at the external perimeter of the IAJ may not necessarily be continuous through to the inner portion of the junction. This observation aligns with findings by Dias et al. [5], who reported that the microgap is intermittent in sectioned samples, suggesting a sinuous and discontinuous path through the IAJ. A recent study found that intermittent smearing of a Au layer can create a continuous mosaic around the connecting surface of the abutment, further contributing to the formation of a tight seal [15].

Bacterial microleakage and dye leakage through the IAJ has traditionally been used to assess and compare the IAJ seal of various implant-abutment combinations [11,18,19]. However, bacterial testing is difficult to quantify precisely due to inherent experimental complexity and limited reproducibility [20,21]. Conversely, a chromophore analysis of dye leakage using UV-Vis spectrometer could enhance quantitative precision and objectivity. Crystal violet would seem an appropriate dye medium as it is extremely stable and non-biodegradable, allowing for analysis to take place over an extended time [22,23].

Given that the abutment material and fabrication method influence the size, morphology and seal of the IAJ, the comparative effects of cast versus milled CoCr abutments and Au surface modifications require investigation. The aims of this study were (1) to design a dye transfer protocol for qualitative and quantitative assessment of IAJ microleakage; (2) to compare the gas and dye leakage of milled Ti, milled CoCr and cast CoCr abutments at the IAJ; (3) to evaluate the effect of Au gilding on the sealing capacity of cast and milled CoCr abutments. The null hypotheses tested were: (i) at the implant–abutment junction, the milled and cast cobalt chrome will exhibit comparable microleakage, and (ii) at the implant–abutment junction, gold-gilded and non-gilded cobalt chrome abutments will exhibit comparable microleakage.

2. Materials and Methods

2.1. Abutment Preparation

A total of 40 abutments were fabricated and equally divided into five groups—milled Ti (MTi), cast CoCr (CCoCr), milled CoCr (MCoCr), cast CoCR with Au gilding (CCoCrG), and milled CoCr with Au gilding (MCoCrG). The abutments used had an external hexagon

connection, a height of 13 mm, and an external diameter of 4 mm (Southern Implants, Irene, South Africa).

The 16 MCoCr abutments were fabricated commercially (Southern Implants, Irene, South Africa). The 16 CCoCr abutments were produced using UCLA plastic burnout abutments (Southern Implants, Irene, South Africa) and a commercially available alloy (Auriloy® Partial, Aurium® Research U.S.A., San Diego, CA, USA) in a commercial laboratory (Sparx Dental, Parramatta, Australia). Eight MTi abutments (Southern Implants, Irene, South Africa) were also used as a control group. Table 1 summarises the studied groups and their characteristics.

Table 1. Summary of studied abutment types.

Group	Sample Size	Abutment Material	Manufacturer
1	8	Milled Ti (MTi)	Southern Implants
2	8	Milled CoCr (MCoCr)	Southern Implants
3	8	Cast Cocr (CCoCr)	Sparx Dental Lab using UCLA plastic abutments supplied by Southern Implants
4	8	Milled CoCr with Au gilding (MCoCrG)	Southern Implants Gold gilding by one investigator
5	8	Cast CoCr with Au gilding (CCoCrG)	Sparx Dental Lab using UCLA plastic abutments supplied by Southern Implants Gold gilding by one investigator

2.2. Au Gilding Technique

Initial attempts at electrodepositing Au onto the CoCr surfaces yielded inconsistent adhesion and film thickness; consequently, a manual gilding technique was adopted. Eight CCoCr and eight MCoCr abutments were cleaned with isopropyl alcohol. A thin coat of oil-based Au size (C.Roberson & Co, London, UK) was painted onto the abutment fitting surface only and left for 3 h as per the supplier's instructions. 24 kt Au 0.12 µm foil was cut into 10 × 10 mm squares and gently placed onto the abutment fitting surface using a bamboo tweezer. Finger pressure was applied to the foil with a sheet of wax paper between. An agate burnisher was then used to burnish the foil to ensure adaptability to the fitting surface. Figure 1 shows a gilded abutment surface after the foil had been placed. Each abutment was assessed and cleaned under a microscope at 20 times magnification to ensure no adhesive or foil was present on the internal surface of the abutment.

Figure 1. This image shows the fitting surface of a milled cobalt chrome abutment after the application of a 23-karat gold 0.12 µm foil layer. The gold foil is manually adapted to the connection geometry prior to assembly and subsequent microleakage testing.

2.3. Implant–Abutment Assembly (IAA)

To ensure experimental consistency and prevent sample mixing, groups were processed and packaged sequentially (MTi, MCoCr, CCoCr, MCoCrG, CCoCrG). Abutments and implants were sequentially allocated and assembled by the primary investigator. To ensure consistency and eliminate selection bias, samples were used and labelled in the order of delivery as provided by the manufacturer.

The forty abutments were attached to regular platform (4.0 mm diameter, 13 mm length) external hexagon implants (Southern Implants, Irene, South Africa), held in a bench-mounted vice. Titanium screws (TSHZ2) (Southern Implants, Irene, South Africa) were torqued to 32 Ncm following the manufacturer's instructions using a manual torque control driver and maintained for 5 s to ensure reliable reproduction of torque force.

2.4. Microleakage Test

The implant–abutment assemblies (IAAs) were connected to a syringe via non-rigid braided silicone tubing (W&H Dentalwek Bürmoos GmbH (Salzburg, Austria)) (Figure 2a). The tubing was pushed over the abutment by 8 mm and into the syringe by 8 mm. A layer of paraffin wax sheet was wrapped around the external surface of the abutment to ensure a good seal.

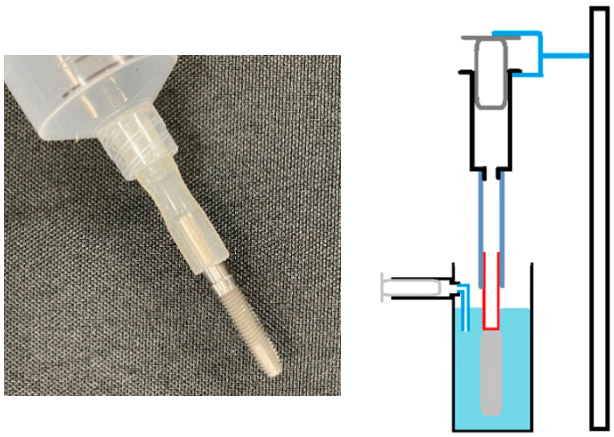

(**a**) (**b**)

Figure 2. (**a**) Assembled components of the experimental setup showing the IAA connected to a 30 mL syringe via non-rigid braided silicone tubing; (**b**) a schematic representation of the set-up. Component colors indicate: blue (tubing), red (abutment), and grey (implant). The assembly is submerged in 60 mL of water on a magnetic stirrer while positive pressure is generated via manual syringe displacement of 6 mL.

2.4.1. Gas Flow Test

The entire experimental set-up was submerged in a beaker containing 60 mL of water, ensuring that the IAJ and rubber tubing connection were submerged (Figure 2b). A gas test was performed for 2 IAAs per group at three different pressures to verify whether the experimental IAAs stayed intact. A 30 mL syringe was held vertically by a clamp with the syringe plunger was depressed by 2 mL, 6 mL and 10 mL to generate the three different pressures and maintained for 10 min. Presence or absence of bubbles at the IAJ was recorded.

The gas leakage test was conducted as a qualitative validation to verify the initial assembly integrity and the presence of a gross seal at the IAJ. Given the exploratory nature of this test and the sample size per group, it was utilised as a binary screening tool (leakage vs. no leakage) rather than for inferential statistical comparison.

2.4.2. Quantitative Dye Leak Test

A serial dilution was performed to create a range of concentrations to establish a calibration curve which was used to determine the concentration of dye released through the IAJ (Figure 3). A starting concentration of 62.5 µg/mL crystal violet (Sigma-Aldrich, St Louis, MO, USA, C.I. 42555; Basic Violet 3) was used and a 1:2 dilution series prepared with water. A plate reader (BMG Labtech CLARIOstar Plus, Ortenberg, Germany) and its proprietary software were used to calibrate and to measure absorption at 590 nm.

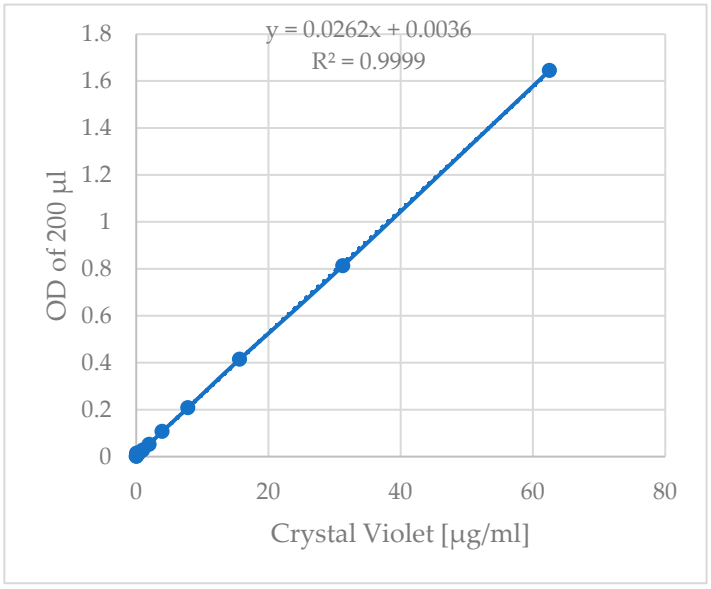

Figure 3. Calibration curve for chromophore analysis. Linear regression analysis showing the relationship between crystal violet absorbance (measured at 590 nm) and dye concentration (µg/mL). This standard curve was used to calculate the quantitative microleakage values from the experimental optical density (O.D.) readings.

A similar experimental set-up to the one used for the gas flow test was used for the dye release test. The syringe contained 30 mL of a 50 µg/mL crystal violet solution (Sigma-Aldrich, C.I. 42555; Basic Violet 3). To initiate the test, the syringe plunger was manually depressed from 30 mL to 24 mL and maintained for 10 min. The volumetric displacement (6 mL) created a hydrostatic pressure intended to drive the dye through any potential microgaps at the IAJ. This method creates a dynamic pressure environment that is characterised by an initial peak followed by a gradual decay over the 10 min testing period. This decay is influenced by the elasticity of the connecting tubing, human variability inherent in manual operation and any leakage of the dye. The whole assembly was set up on top of a magnetic stirrer to ensure a more homogenous sampling and prevent the dye from settling.

To evaluate the leakage, a sample of 200 µL was taken from the reservoir (60 mL) using a pipette (Transferpette®, Brand GmbH + Co KG (Wertheim, Germany) every minute for 10 min and transferred to a 96-well microplate for spectrophotometry analysis (BMG Labech CLARIOstar Plus, Ortenberg, Germany). Dye leak analysis data were used to evaluate the effectiveness of sealing at the implant–abutment junction.

The primary investigator connected all the IAAs and performed all the laboratory operations under the same conditions. A secondary investigator performed the quantitative spectrometer analysis. All data were recorded using a standardised software-driven protocol to ensure objective acquisition of absorbance values.

Following spectrophotometry, a verification protocol was implemented to ensure data integrity. All microplate wells were examined under a digital stereomicroscope to

distinguish true chromophore concentration from physical artefacts. Specific data points were excluded from the final analysis if they exhibited anomalous absorbance peaks attributed to identifiable artefacts, defined as: (i) air bubbles, (ii) physical scratches on the external base of the microplate well, or (iii) non-dye particulate contamination (e.g., environmental dust or microscopic fibrous debris). This ensured that the reported values exclusively represented true microleakage, preventing the inclusion of false-positive readings caused by physical contaminants.

Baseline corrections were performed by including control wells which were empty and containing water only and were scanned simultaneously with the experimental samples. The mean absorbance value of the water-only controls was calculated and subtracted from all sample readings of the corresponding microplate to account for the background absorbance. Using the absorption values, the dye concentration was calculated using the formula generated by the standard curve.

A sample was classified as having confirmed leakage if the calculated concentration exceeded the baseline detection threshold (established by the mean water-only absorbance) and the absence of physical artefacts. Samples meeting these criteria were included in the leakage incidence and any resulting negative concentration values—arising from the calculations—were interpreted as zero leakage.

2.5. Statistical Analysis

Binary leakage data (leak vs. no leak) were assessed using the Fisher exact test. For quantitative dye leakage, descriptive statistics including medians and interquartile Ranges (IQRs) were calculated to provide a representative summary of group performance. To evaluate the total magnitude of dye penetration over the 10 min interval the Area Under the Curve (AUC) was calculated for each sample using the trapezoidal rule.

The data were split to compare the manufacturing effect and the Au effect: (i) MCoCr (Group 2) vs. CCoCr (Group 3), and (ii) CCoCr (Group 3) vs. CCoCrG (Group 5). Results were considered significant at $p < 0.05$. Sample size ($n = 8$) was verified via post hoc power analysis.

2.6. Scanning Electron Microscopy (SEM) Examination

The connecting abutment surfaces from each group were assessed prior to implant connection using a scanning electron microscope (SEM) (Phenom XL G2 Desktop SEM, ThermoFisher Scientific, Waltham, MA, USA, and JEOL SEM 840, Tokyo, Japan). Two microscopy experts (Institute of Dental Research, Westmead Centre for Oral Health, Westmead, NSW, Australia) (Arto Hardy Family Biomedical Innovation Hub, Chris O'Brien Lifehouse, Camperdown, NSW, Australia) performed the assessments. Once connected, the external perimeters of the IAJs were assessed.

SEM analysis was conducted for the illustrative visualisation of surface morphology and interfacial adaptation. SEM images were not utilised for linear microgap quantification; instead, they serve to provide qualitative context for the physical disparities observed between the milled and cast groups.

3. Results

3.1. Presence or Absence of Gas Flow at the Implant–Abutment Junction (IAJ)

All IAAs maintained integrity throughout this qualitative experiment. Some samples showed bubbling at the IAJ indicative of gas escape through the microgap (Figure 4a,b). As this initial assessment served primarily to confirm integrity of the assembly, the findings are reported descriptively in Table 2.

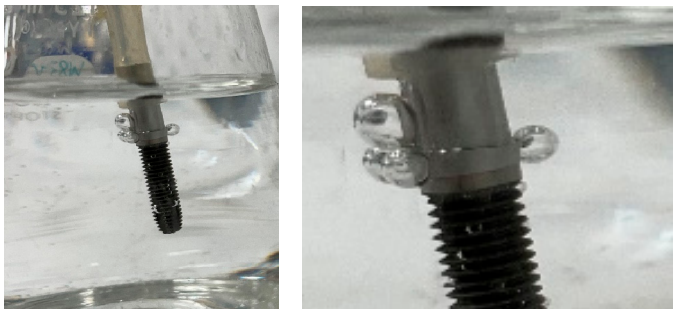

(**a**) (**b**)

Figure 4. Qualitative gas leakage validation at the IAJ. Gas leakage during testing: (**a**) MCoCr (Group 2) abutment sample A submerged during the 10 mL piston displacement test. (**b**) Higher magnification view of the IAJ, clearly showing the formation of gas bubbles escaping through the microgap. Bubbling indicates microleakage.

Table 2. Qualitative evaluation of gas microleakage at the IAJ.

	MTi		MCoCr		CCoCr		MCoCrG		CCoCrG	
Sample / **Piston Level**	**A**	**B**	**A**	**B**	**A**	**B**	**A**	**B**	**A**	**B**
28 mL	Seal	Seal	Seal	Seal	Seal	Seal	Seal	Seal	Seal	Seal
24 mL	Seal	Seal	Seal	Seal	Leak	Leak	Seal	Seal	Seal	Seal
20 mL	Seal	Seal	Leak	Seal	Leak	Leak	Seal	Seal	Seal	Seal

Note: Results represent binary assessment (Seal vs. Leakage) of assembly integrity during positive pressure application via manual syringe displacement. A result of "Seal" indicates no observable gas escape, while "Leak" indicates the presence of bubbling at the interface. Groups: MTi (Group 1), MCoCr (Group 2), CCoCr (Group 3), MCoCrG (Group 4), and CCoCrG (Group 5).

3.2. Dye Leak Test

The 40 IAAs were compared for dye leakage. The raw data (optical density [O.D.]) from the plate reader were converted to dye concentrations using the equation developed from the concentration curve (Figure 3). The experimental data and corresponding calculations are graphically represented in Figure 5a–e below.

To ensure the accuracy of the microleakage profiles, all samples underwent a microscopic verification protocol. A total of 400 data points (80 per group across 10 time points) were initially recorded. Based on the microscopic exclusion criteria, 25 points were removed due to the confirmed physical artefacts. The exclusion of data points was randomly distributed across different time points and specimens, comprising Group 1: n = 17 (21.25% excluded); Group 2: n = 6 (7.5% excluded); Group 3: n = 2 (2.5% excluded). Table 3 summarises the results of the number of samples with dye leakages.

Table 3. Summary of results of dye test.

Group	Abutment	Number of Samples with Dye Leakages	Leakage Frequency
1	MTi	0/8	0%
2	MCoCr	0/8	0%
3	CCoCr	5/8	62.5%
4	MCoCrG	0/8	0%
5	CCoCrG	2/8	25%

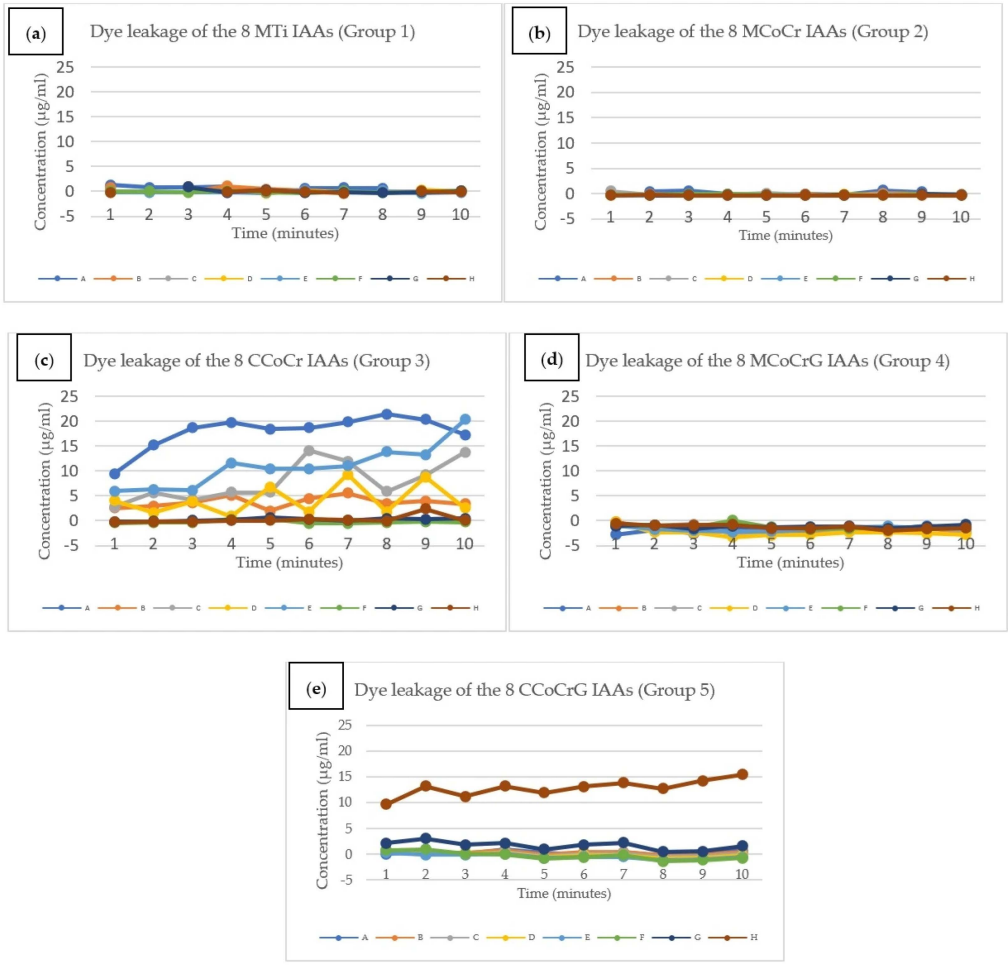

Figure 5. Quantitative microleakage profiles over a 10 min testing interval. Graphs represent crystal violet concentration (µg/mL) detected in the external reservoir for: (**a**) MTi (Group 1), (**b**) MCoCr (Group 2), (**c**) CCoCr (Group 3), (**d**) MCoCrG (Group 4), and (**e**) CCoCrG (Group 5). Groups 1, 2, and 4 demonstrated no microleakage, whereas the non-gilded cast group (Group 3) (**c**) showed the highest leakage. The colored lines (A–H) represent the eight individual samples tested within each group, with consistent color-coding used across all graphs. Note: The small negative values observed on the *y*-axis are a mathematical artefact and these values indicate zero dye leakage.

Statistical analysis revealed a significant difference in dye leakage frequency between MCoCr (Group 2) and CCoCr (Group 3). The Fisher exact test yielded a p-value of 0.026 (Odds Ratio [OR] 95% CI: 1.325 to ∞). In contrast, the comparison between CCoCr (Group 3) and CCoCrG (Group 5) did not reach statistical significance ($p = 0.315$, OR 95% CI: 0.013 to 2.447), despite an observed reduction in leakage frequency from 62.5% to 25%.

A sensitivity analysis was conducted to evaluate the impact of transient baseline spikes. Even if these spikes were treated as true leakage events (resulting in a frequency of 2/8 for Group 2 and 7/8 for Group 3), the impact of the fabrication method on seal integrity remained statistically significant ($p = 0.041$). However, because these spikes represent a physical impossibility within a cumulative leakage model, they were excluded from the primary analysis to ensure results were restricted to verified, sustained leakage events ($p = 0.026$).

To evaluate the magnitude of dye penetration across the groups, Medians, IQR and AUC were utilised. While the 10 min concentration identifies the endpoint leakage, the AUC serves as an integrated metric that captures the total cumulative penetration throughout the experimental window. These descriptors (Table 4) provide a more representative interpretation of the leakage profiles.

Table 4. Quantitative descriptors of dye leakage concentration (μg/mL) at 10 min.

Group	Abutment	Median Final Dye Concentration (μg/mL)	Interquartile Range (IQR) (25–75th) (μg/mL)	Median Total AUC (μg·min/mL)	Total AUC Interquartile Range (IQR) (μg·min/mL)
1	MTi	0.00	0.00–0.00	0.00	0.00–0.00
2	MCoCr	0.00	0.00–0.00	0.00	0.00–0.00
3	CCoCr	2.95	0.27–15.48	37.74	2.48–85.64
4	MCoCrG	0.00	0.00–0.00	0.00	0.00–0.00
5	CCoCrG	0.00	0.00–1.54	1.38	0.00–10.13

Although the comparison of leakage frequency between Group 3 and Group 5 did not reach statistical significance ($p = 0.315$), the quantitative descriptors provide additional context regarding the scale of dye penetration. The median concentration for Group 3 was 2.95 μg/mL (IQR: 0.27–15.48), whereas Group 5 exhibited a median of 0.00 μg/mL (IQR: 0.00–1.54). These observations suggest that the application of Au may influence the total volume of dye penetration. Such descriptive data highlight differences in leakage magnitude that are not fully captured by binary frequency analysis alone.

3.3. Scanning Electron Microscope (SEM) Examination

SEM images of the abutment connection surface from Groups 1–5 were assessed prior to assembly (Figures 6–8) and revealed distinct morphological differences between the groups. These images are presented as illustrative representations of the interface rather than quantitative measurements of the microgap. The CCoCr surface (Figure 6c) shows significant irregularities on the surface compared to the MTi and MCoCr surfaces (Figure 6a,b). The 38 times magnification of three samples each of Au gilded surfaces of MCoCrG and CCoCrG are shown in Figures 7 and 8.

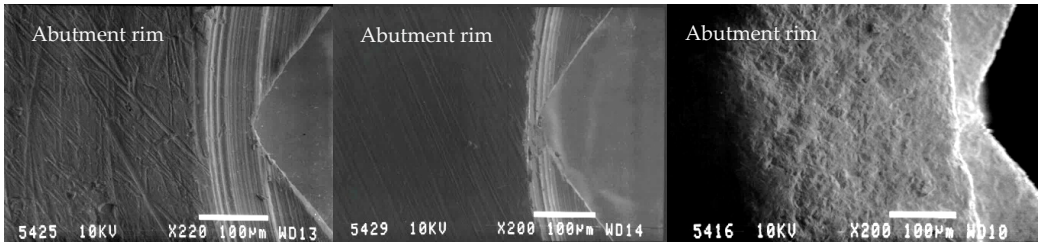

(**a**) (**b**) (**c**)

Figure 6. The 200× magnification view of abutment connection surface: (**a**) MTi (Group 1, Abutment A), (**b**) MCoCr (Group 2, Abutment A) and (**c**) CCoCr (Group 3, Abutment A). Size bar: 100 μm.

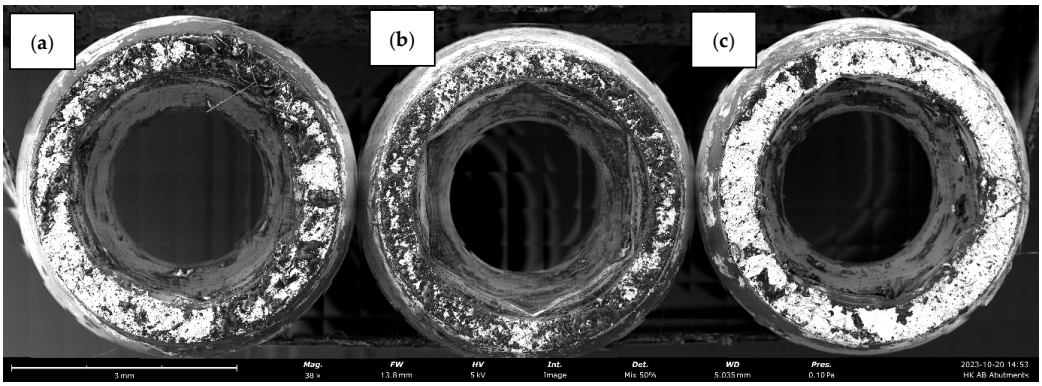

Figure 7. The 38× magnification of MCoCrG (Group 4) abutment connection surfaces, (**a**) Abutment A, (**b**) Abutment B, (**c**) Abutment C. Size bar: 3 mm.

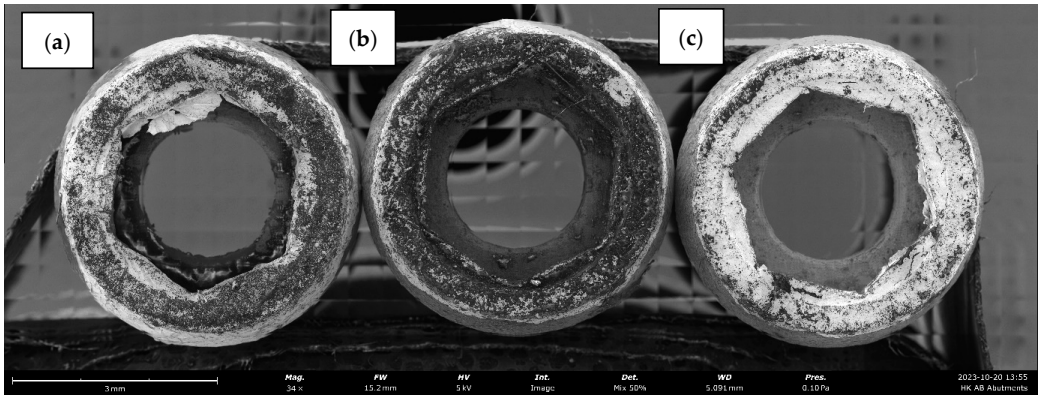

Figure 8. The 34× magnification of CCoCrG (Group 5) abutment connection surfaces, (**a**) Abutment sample A, (**b**) Abutment sample B, (**c**) Abutment sample C. Size bar: 3 mm.

Once connected, the external perimeter of each of the IAJ microgaps was imaged (Figure 9). The MTi (Group 1) (Figure 9a) and MCoCr (Group 2) (Figure 9b) show close contact. The CCoCr (Group 3) shows irregularities and a discernible gap at the junction (Figure 9c).

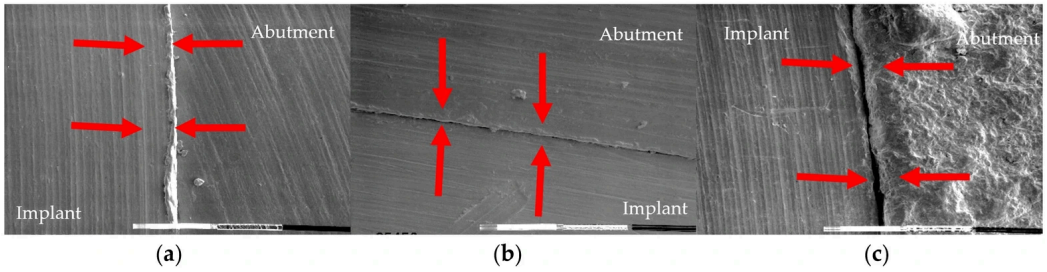

Figure 9. SEM images of the IAJ external perimeter (200× magnification). (**a**) MTi (Group 1) and (**b**) MCoCr (Group 2) showing close contact at the interface. (**c**) CCoCr (Group 3) exhibiting surface irregularities and a discernible microgap (identified by arrows).

The addition of Au to the abutment appears to have filled the space at these gaps (Figure 10). This adaptation observed at the external perimeter suggests a narrowing of the microgap, which may contribute to the directional improvement in sealing performance depicted in of Figure 5c,e.

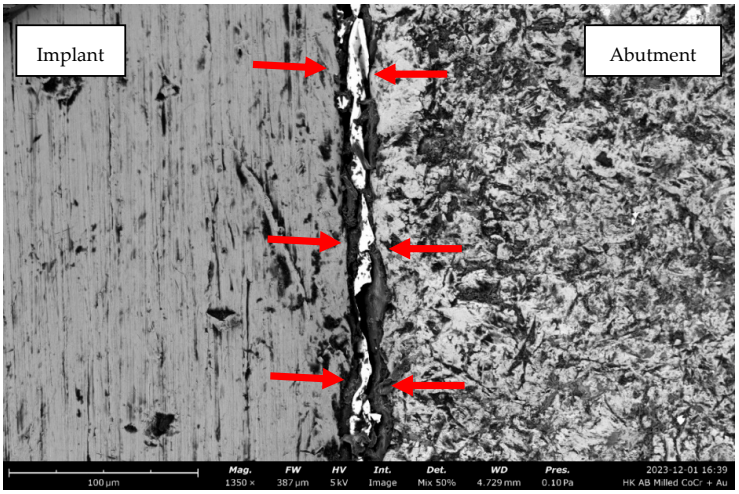

Figure 10. The 1350× magnified view of the IAJ external perimeter of MCoCrG (Group 4, Abutment sample A). The high-density gold interspersed in the gap is identified by the arrows. Size bar: 100 µm.

After the dye leak test was conducted, the IAAs were disassembled, and surface topography was assessed again and compared to the surface topography before torque application. Figure 11a,b shows the Au-gilded surface of Abutment A from Group 5 before and after torque application. The "white" areas represent the Au layer. The before and after photos show a change in the surface, indicating plastic deformation of the Au with torque application.

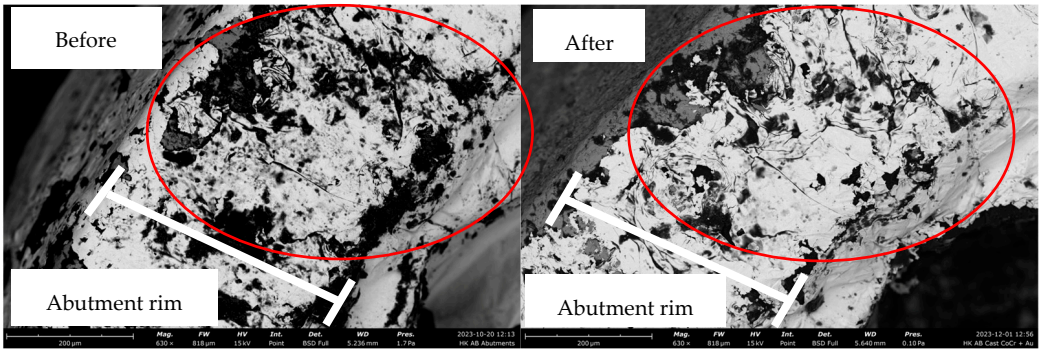

(**a**) (**b**)

Figure 11. SEM images of the CCoCrG (Group 5) abutment connection surface (magnification 630×) showing deformation of the gold leaf. (**a**) View of the abutment rum before torque application; (**b**) view of the same area after torque application. The images highlight the physical change and deformation of the gold layer (encircled area) upon assembly, which is indicative of plastic deformation and filling of microgap. Size bar: 200 µm.

4. Discussion

The null hypotheses were partially rejected as the fabrication method exerted a statistically significant effect on seal integrity (p = 0.026). However, the comparison of cast with and without Au did not reach statistical significance (p = 0.315). While this specific variable did not meet the threshold for significance, the observed reduction in leakage frequency suggests a clinical trend that warrants further investigation with a larger cohort. Furthermore, the quantitative analysis revealed a substantial reduction in the total magnitude of dye penetration, suggesting that the Au gilding treatment provides improved resistance to cumulative dye leakage.

In this in vitro study, the microleakage of Ti and CoCr abutments, both cast and milled, was investigated under static conditions. Cast CoCr showed the most leakage when compared to the other abutments. Milled Ti and milled CoCr abutments with and without Au gilding did not show any leakage. The Au gilded cast CoCr abutments showed decreased leakage frequency compared to the cast CoCr abutments.

The use of crystal violet as a staining agent for microleakage evaluation at the IAJ has not been previously reported for this specific application as most studies use methylene blue or bacteria models. Crystal violet, being extremely stable and non-biodegradable, allows for analysis to take place over an extended time [22,23]. This contrasts with methylene blue, which is more susceptible to photodegradation, potentially leading to inaccurate quantitative measurements over long observation periods [24]. While bacterial leakage models are clinically relevant, they are often qualitative outcomes; even when colony forming units (CFUs) are counted, this process is prone to high manual error [20,21]. By utilising a dye-based approach with UV-Vis spectrometer and chromophore analysis, this study eliminates the inherent variability associated with biological growth rates, providing a precise, reproducible assessment of the physical seal at the IAJ.

The pre-test SEMs showed that significant irregularities existed at the cast CoCr fitting surface, with a larger microgap viewed externally compared to the milled Ti and milled CoCr samples (Figure 9a–c). This is consistent with what is known about a multi-step lost-wax casting process in which irregularities are introduced into the geometry at the junction. The casting process is largely dependent on the technician's skill and the quality of the alloy. These findings were consistent with those of Molinero-Mourelle et al. [10], who found that cast CoCr abutments had more microleakage than milled CoCr abutments. However, not all the cast abutment samples leaked; three out of eight abutments in Group 3 maintained a seal, highlighting the inconsistencies between the samples and variations in the casting process.

The results of this study have shown that material type and fabrication technique have an impact on the IAJ microleakage. It is widely accepted that milled abutments with fewer surface disparities result in smaller microgaps than cast surfaces [25–27]. The result of the current study suggests this with both the milled-Ti and milled-CoCr IAAs showing no microleakage.

The addition of Au to the cast abutment connecting surface was associated with a lower frequency of microleakage. Only two of the cast CoCr abutments with Au gilding leaked compared to five of the cast CoCr abutments without Au gilding. The addition of Au at the junction is thought to fill in the voids around the microscopic disparities arising from the casting processes. This is reflected in the reduced leakage detected by the plate reader and is consistent with results obtained in a previous study where cast high-Au content alloys were used [15].

Even though vertical misfit was visible on the cast cobalt chrome with Au gilding, no leakage was detected by the spectrometer for six of the eight samples. This could be because a vertical misfit at the outer edge of the junction may not be continuous from the outer edge to the inner portion of the junction as previously discussed [5]. This is also consistent with a recent study which showed intermittent smearing of the Au layer with potential formation of a continuous mosaic barrier around the connecting surface of the abutment [15] potentially mitigating leakage and enhancing the seal as suggested by the results shown in Figures 5e and 10.

The use of external hexagon implants for this study facilitated the ease in the application of the Au layer on to the flat abutment connecting surface. Additionally, the flat surface facilitates visibility under SEM. These factors are difficult with internal connections and for SEM would likely require sectioning. If the seal can be achieved with external hexagon connections, it is likely it can be achieved with internal connections, provided that the abutments can be adequately seated.

The degree of microleakage is a multifactorial condition that is dependent on factors such as precision of fit between the connected components, the degree of micromovement between the components, and the amount of clamping force holding the components together.

Micromovement is an important factor because it can facilitate bacterial movement and associated metabolic products across the IAJ, leading to increased concentrations from within the internal screw chamber and mucosal cuff. This is known to initiate a zone of inflammation adjacent to the IAJ, which can lead to both horizontal and vertical bone loss [6] and contribute to future biological and technical complications [28].

This study has several limitations that should be addressed in future research. The primary limitation is the lack of cyclical loading assessment. While our results suggest that the Au-gilded surface is associated with a lower leakage frequency, the potential for micromovement under cyclic loading to disrupt or eliminate this gilded layer and affect

its sealing capacity over time remains an area of investigation. Additionally, the limited sample size precluded more robust statistical analysis.

The pressure applied during the gas and dye leakage test was via manual syringe displacement, which represents a transient pressure model. This approach introduces variables such as tubing elasticity and manual variability, which may lead to a peak and decay pressure profile over the 10 min testing interval. Furthermore, in samples where leakage occurred, the resulting volume loss within the assembly likely contributed to a further decrease in pressure. This manual approach lacks the precision of electronic pressure transducers. To improve quantitative reproducibility, future studies should utilise calibrated pressure regulators and real-time monitoring throughout the testing duration.

The gold-gilding technique employed in this study serves as a conceptual demonstration of the 'gold gasket' effect. It is acknowledged that the manual burnishing of 0.12 µm Au foil does not produce a standardised coating thickness or perfectly uniform surface coverage. While this method suggests the potential for a malleable layer to favourably influence the seal of cast interfaces, further research using standardised electroplating or vacuum-deposition techniques is required to quantify the ideal coating thickness and durability for clinical translation.

Within the limitations of the study, the following can be concluded:

1. The use of chromophore analysis using crystal violet proved to be a viable method in assessing the quantitative analysis of leakage across the IAJ.
2. Microleakage varied and was influenced by the abutment material and fabrication method. Under the tested conditions, milled Ti and milled CoCr abutments demonstrated superior leakage resistance compared to cast CoCr abutments.
3. The addition of Au to the abutment fitting surface was associated with a numerical reduction in leakage frequency and volume, suggesting a potential compensatory effect when an ideal fit is not achieved.

These findings represent initial outcomes in a static environment; further research incorporating cyclic loading and long-term ageing is required to determine the clinical durability of these seals.

Author Contributions: Conceptualization, A.K.B. and T.R.W.; methodology, A.K.B. and T.R.W.; validation, A.K.B. and T.R.W.; formal analysis, A.K.B.; investigation, A.K.B.; resources, A.K.B.; data curation, A.K.B. and H.V.K.; writing—original draft preparation, A.K.B. and T.R.W.; writing—review and editing, A.K.B. and T.R.W.; visualisation, A.K.B.; supervision, T.R.W. and D.G.H.; project administration, A.K.B.; funding acquisition, A.K.B. All authors have read and agreed to the published version of the manuscript.

Funding: This research was financially supported by the Australasian Osseointegration Society (AOS) NSW Branch and the Australian Prosthodontic Society (APS) Federal. The funders had no role in the design of the study; in the collection, analyses, or interpretation of data; in the writing of the manuscript; or in the decision to publish the results.

Institutional Review Board Statement: Not applicable.

Informed Consent Statement: Not applicable.

Data Availability Statement: The original contributions presented in this study are included in the article. Further inquiries can be directed to the corresponding author.

Acknowledgments: The authors would like to thank all funders, Jinlong Gao (The University of Sydney), Mara Cvejic (Institute of Dental Research, Westmead Centre for Oral Health), Jeremy Crook and Linda Rogers (Arto Hardy Family Biomedical Innovation Hub, Chris O'Brien Lifehouse) for their assistance in this study. The authors would like to acknowledge Southern Implants for the contribution of implant componentry used in this study.

Conflicts of Interest: The authors declare no conflicts of interest.

Abbreviations

The following abbreviations are used in this manuscript:

IAJ	Implant–abutment junction
IAA	Implant–abutment assembly
Ti	Titanium
Au	Gold
CoCr	Cobalt chrome
MCoCr	Milled cobalt chrome
CCoCr	Cast cobalt chrome
MCoCrG	Milled cobalt chrome with gold gilding
CCoCrG	Cast cobalt chrome with gold gilding
Zi	Zirconia
SEM	Scanning electron microscope
CAD/CAM	Computer-aided design/computer aided
O.D.	Optical density
IQR	Interquartile Range
AU	Area Under the Curve
CFU	Colony Forming Unit

References

1. Pjetursson, B.E.; Asgeirsson, A.G.; Zwahlen, M.; Sailer, I. Improvements in implant dentistry over the last decade: Comparison of survival and complication rates in older and newer publications. *Int. J. Oral Maxillofac. Implants* **2014**, *29*, 308–324. [CrossRef]
2. Walton, T.R. The up-to-14-year survival and complication burden of 256 TiUnite implants supporting one-piece cast abutment/metal-ceramic implant-supported single crowns. *Int. J. Oral Maxillofac. Implants* **2016**, *31*, 1349–1358. [CrossRef]
3. Ozdiler, A.; Bakir-Topcuoglu, N.; Kulekci, G.; Isik-Ozkol, G. Effects of taper angle and sealant agents on bacterial leakage along the implant-abutment interface: An in vitro study under loaded conditions. *Int. J. Oral Maxillofac. Implants* **2018**, *33*, 1071–1077. [CrossRef]
4. Tripodi, D.; D'Ercole, S.; Iaculli, F.; Piattelli, A.; Perrotti, V.; Iezzi, G. Degree of bacterial microleakage at the implant-abutment junction in cone morse tapered implants under loaded and unloaded conditions. *J. Appl. Biomater. Funct. Mater.* **2015**, *13*, e367–e371. [CrossRef]
5. Dias, E.C.; Bisognin, E.D.; Harari, N.D.; Machado, S.J.; da Silva, C.P.; Soares, G.D.; Vidigal, G.M., Jr. Evaluation of implant-abutment microgap and bacterial leakage in five external-hex implant systems: An in vitro study. *Int. J. Oral Maxillofac. Implants* **2012**, *27*, 346–351.
6. Broggini, N.; McManus, L.M.; Hermann, J.S.; Medina, R.U.; Oates, T.W.; Schenk, R.K.; Buser, D.; Mellonig, J.T.; Cochran, D.L. Persistent acute inflammation at the implant-abutment interface. *J. Dent. Res.* **2003**, *82*, 232–237. [CrossRef]
7. Khorshidi, H.; Raoofi, S.; Moattari, A.; Bagheri, A.; Kalantari, M.H. In vitro evaluation of bacterial leakage at implant-abutment connection: An 11-degree morse taper compared to a butt joint connection. *Int. J. Biomater.* **2016**, *2016*, 8527849. [CrossRef] [PubMed]
8. Baggi, L.; Di Girolamo, M.; Mirisola, C.; Calcaterra, R. Microbiological evaluation of bacterial and mycotic seal in implant systems with different implant-abutment interfaces and closing torque values. *Implant Dent.* **2013**, *22*, 344–350. [CrossRef] [PubMed]
9. Assenza, B.; Tripodi, D.; Scarano, A.; Perrotti, V.; Piattelli, A.; Iezzi, G.; D'Ercole, S. Bacterial leakage in implants with different implant-abutment connections: An in vitro study. *J. Periodontol.* **2012**, *83*, 491–497. [CrossRef] [PubMed]
10. Molinero-Mourelle, P.; Cascos-Sanchez, R.; Yilmaz, B.; Lam, W.; Pow, E.; Río, J.; Gomez-Polo, M. Effect of fabrication technique on the microgap of CAD/CAM cobalt-chrome and zirconia abutments on a conical connection implant: An in vitro study. *Materials* **2021**, *14*, 2348. [CrossRef]
11. Naser Mostofy, S.; Jalalian, E.; Valaie, N.; Mohtashamrad, Z.; Haeri, A.; Bitaraf, T. Study of the effect of GapSeal on microgap and microleakage in internal hex connection after cyclic loading. *J. Res. Dent. Maxillofac. Sci.* **2019**, *4*, 36–42. [CrossRef]
12. Fernandes, P.F.; Grenho, L.; Fernandes, M.H.; Sampaio-Fernandes, J.C.; Sousa Gomes, P. Microgap and microleakage of a hybrid connection platform-switched implant system in the absence or presence of a silicone-based sealing agent. *Odontology* **2022**, *110*, 231–239. [CrossRef]
13. Hunt, L.B. The long history of lost wax casting. *Gold Bull.* **1980**, *13*, 63–79. [CrossRef]

14. de França, D.G.B.; Morais, M.H.S.T.; das Neves, F.D.; Barbosa, G.A.S. Influence of CAD/CAM on the fit accuracy of implant-supported zirconia and cobalt-chromium fixed dental prostheses. *J. Prosthet. Dent.* **2015**, *113*, 22–28. [CrossRef]
15. Walton, T.R. Effect of electrodeposited gold coatings on micro-gaps, surface profile and bacterial leakage of cast UCLA abutments attached to external hexagon dental implants. *Coatings* **2023**, *13*, 1976. [CrossRef]
16. Silva, M.D.; Walton, T.R.; Alrabeah, G.O.; Layton, D.M.; Petridis, H. Comparison of corrosion products from implant and various gold-based abutment couplings: The effect of gold plating. *J. Oral Implantol.* **2021**, *47*, 370–379. [CrossRef]
17. Papathanasiou, I.; Dimitriadi, M.; Zinelis, S. Surface, microstructural, and mechanical characterization of abutment screws with modified surface characteristics. *J. Esthet. Restor. Dent.* **2025**, *37*, 2207–2219. [CrossRef] [PubMed]
18. Berberi, A.; Tehini, G.; Rifai, K.; Bou Nasser Eddine, F.; El Zein, N.; Badran, B.; Akl, H. In vitro evaluation of leakage at implant-abutment connection of three implant systems having the same prosthetic interface using rhodamine B. *Int. J. Dent.* **2014**, *2014*, 351263. [CrossRef] [PubMed]
19. D'Ercole, S.; Dotta, T.C.; Farani, M.R.; Etemadi, N.; Iezzi, G.; Comuzzi, L.; Piattelli, A.; Petrini, M. Bacterial microleakage at the implant-abutment interface: An in vitro study. *Bioengineering* **2022**, *9*, 277. [CrossRef]
20. Trinh, K.T.L.; Lee, N.Y. Recent methods for the viability assessment of bacterial pathogens: Dvances, challenges, and future perspectives. *Pathogens* **2022**, *11*, 1057. [CrossRef]
21. Hombach, M.; Ochoa, C.; Maurer, F.P.; Pfiffner, T.; Böttger, E.C.; Furrer, R. Relative contribution of biological variation and technical variables to zone diameter variations of disc diffusion susceptibility testing. *J. Antimicrob. Chemother.* **2016**, *71*, 141–151. [CrossRef]
22. Tian, Y.; Wu, K.; Lin, S.; Shi, M.; Liu, Y.; Su, X.; Islam, R. Biodegradation and decolorization of crystal violet dye by cocultivation with fungi and bacteria. *ACS Omega* **2024**, *9*, 7668–7678. [CrossRef]
23. Kwak, S.J.; Park, J.; Sim, Y.; Choi, H.; Cho, J.; Lee, Y.-M. Biodegradation of crystal violet by newly isolated bacteria. *PeerJ* **2024**, *12*, e17442. [CrossRef]
24. Ali, M.A.; Maafa, I.M.; Qudsieh, I.Y. Photodegradation of methylene blue using a UV/H_2O_2 irradiation system. *Water* **2024**, *16*, 453. [CrossRef]
25. Byrne, D.; Houston, F.; Cleary, R.; Claffey, N. The fit of cast and premachined implant abutments. *J. Prosthet. Dent.* **1998**, *80*, 184–192. [CrossRef]
26. Lalithamma, J.J.; Mallan, S.A.; Murukan, P.A.; Zarina, R. A comparative study on microgap of premade abutments and abutments cast in base metal alloys. *J. Oral Implantol.* **2014**, *40*, 239–249. [CrossRef] [PubMed]
27. Molinero-Mourelle, P.; Roccuzzo, A.; Yilmaz, B.; Walter Pow, E.H.N.; Highsmith, J.D.R.; Gómez-Polo, M. Microleakage assessment of CAD-CAM cobalt-chrome and zirconia abutments on a conical connection dental implant: A comparative in vitro study. *Clin. Oral Implants Res.* **2022**, *33*, 945–952. [CrossRef] [PubMed]
28. Liu, Y.; Wang, J. Influences of microgap and micromotion of implant-abutment interface on marginal bone loss around implant neck. *Arch. Oral Biol.* **2017**, *83*, 153–160. [CrossRef] [PubMed]